The effect of fuel droplets on the burning velocity of strained laminar acetone/air flames

McGrath, Dante; Fan, Luming; Gkantonas, Savvas; Hochgreb, Simone

Publisher's version / Version de l'éditeur:
https://doi.org/10.1016/j.proci.2022.07.133
Proceedings of the Combustion Institute, 39, 2, pp. 2503-2511, 2022-09-13

Available online at www.sciencedirect.com

ScienceDirect

Proceedings of the Combustion Institute 39 (2023) 2503–2511

Proceedings of the Combustion Institute

www.elsevier.com/locate/proci

The effect of fuel droplets on the burning velocity of strained laminar acetone/air flames

Dante McGrath [a,*], Luming Fan [a,b], Savvas Gkantonas [a], Simone Hochgreb [a]

[a] *Department of Engineering, University of Cambridge, Trumpington Street, Cambridge, CB2 1PZ, United Kingdom*
[b] *Aerospace Research Centre, National Research Council Canada, 1200 Montreal Road, Ottawa, K1A 0R6, Canada*

Received 9 December 2021; accepted 12 July 2022
Available online 13 September 2022

Abstract

The effect of fuel droplets on the burning velocity of strained laminar premixed flames is investigated via experimentation and simulation. The twin counterflow configuration was used to obtain reference flame speeds as a function of strain rate for a prevaporized flame and a dilute spray flame simultaneously, both composed of acetone and air. The mixtures were varied with respect to nominal equivalence ratio (0.8–1.4) and strain rate (200–600 s^{-1}). Gas velocities were measured using particle image velocimetry. Droplet size, velocity, and concentration were measured using phase Doppler anemometry: non-reacting flow measurements were taken at a position upstream of the stagnation plane; reacting flow measurements were taken along the stagnation streamline. The droplet Sauter mean diameter ranged between 65–75 μm, and the estimated fuel liquid fraction varied between 6–22%, increasing with nominal equivalence ratio. The results show that the reference flame speed of the spray flame decreases slightly relative to that of the prevaporized flame in the case of lean mixtures, but appears unchanged in the case of stoichiometric and rich mixtures. Gas velocity profiles and droplet measurements along the stagnation streamline suggest that the spray flame vaporization is incomplete, such that the reference flame speed corresponds to that of a lower equivalence ratio. Conversely, the opposing flame is affected by the fraction of droplets that do not vaporize in the spray flame and either penetrate the flame front, causing fuel enrichment, or evaporate near the stagnation plane, reducing the adiabatic flame temperature. The effect appears primarily for rich mixtures with higher liquid fraction, as evidenced by the lower reference flame speed and lower axial velocity rise across the flame. This study provides a systematic framework to examine the influence of fuel droplets on laminar flame propagation using a single-component fuel in the counterflow configuration.

Keywords: Droplets; Laminar flame speed; Counterflow; Acetone

* Corresponding author.
E-mail address: dm771@cantab.ac.uk (D. McGrath).

https://doi.org/10.1016/j.proci.2022.07.133

1. Introduction

Spray combustion is used in a variety of devices. A typical goal is to produce micron-sized droplets of well-mixed liquid fuels to produce clean and nearly premixed combustion. The present study examines how fuel droplets affect the burning velocity of strained laminar premixed flames. A number of experimental studies have investigated the effect of fuel and inert droplets in quasi-laminar premixed combustion. Hayashi et al. [1] examined the effect of ethanol and *n*-octane droplets on the propagation of spherical flames through stagnant reactant mixtures in a closed combustion chamber; they found that a higher liquid fraction of fuel caused a significant temperature drop due to latent heat, culminating in a decreased overall reaction rate. Nomura et al. [2] performed similar experiments with 11 μm diameter ethanol droplets under microgravity, to show that the laminar flame speed curve as a function of equivalence ratio shifts to leaner values; the overall reaction rate increased at lean values and decreased at rich values relative to the vapor mixtures. Ballal and Lefebvre [3] used a constant pressure chamber with spherical flame propagation to show that the laminar flame speed of a droplet-laden mixture decreased relative to that of a pure vapor mixture for increased droplet size (30–150 μm) in lean and stoichiometric mixtures of air and either iso-octane, diesel oil or heavy fuel oil. The same study posited that, for lean to stoichiometric mixtures, flame speed is enhanced as gas density, fuel volatility, and vapor fraction are increased.

A number of computational studies have been performed on the counterflow, one-dimensional, non-premixed configuration to include droplets. Chelliah [4] investigated the effect of water droplets on the extinction of both premixed and non-premixed methane/air flames, finding optimal water droplet sizes which maximize the effect of extinction. Kee et al. [5] simulated non-premixed flames with small droplets (< 10 μm), finding that *n*-heptane droplets evaporated prior to entering the flame, while less volatile diesel fuel droplets survived up to the edge of the flame. More recently, Franzelli et al. [6] proposed a generalized mixture fraction approach for non-premixed spray flames.

Neophytou and Mastorakos [7] simulated the propagation of unstrained adiabatic premixed flames in the presence of droplets, and found that the maximum flame speed for an *n*-heptane mixture occurred with small droplets (< 10 μm) for lean conditions and relatively large droplets (> 30 μm) for rich conditions, as suggested in the experimental work of Ballal and Lefebvre [3]. However, such findings have yet to be rigorously validated by corresponding experiments.

Our previous work used the impinging jet configuration for premixed methane/air mixtures to examine the effect of small acetone droplets (1–5 μm) on flame propagation, as compared to the corresponding vapor mixture [8]. The reference flame speed, measured using particle image velocimetry (PIV), was lowered by droplets under lean conditions, and enhanced under rich conditions. The two factors cited to affect the flame speed were the effective equivalence ratio associated with the vaporized droplets and the mixture temperature. On the lean side, both a lower equivalence ratio and mixture temperature contributed to lower the flame speed; on the rich side, the temperature was lower, but the lower effective equivalence ratio increased the flame speed. The wall-impinging flames considered in the original study could not be stabilized with pure acetone fuel and droplets at ambient conditions owing to heat losses to the wall, which is why a hybrid mixture of methane and acetone was chosen.

In the present study, the difficulty from that prior configuration [8,9] is overcome using a twin, premixed, counterflow configuration. This allows the use of a single fuel (acetone) in quasi-adiabatic, quasi-one-dimensional conditions. The configuration was operated in two modes: dual-prevaporized and prevaporized/spray, both containing premixed acetone/air mixtures. In this system, either both flames are fully vaporized as the baseline case, or one of the flames is seeded with droplets with Sauter mean diameters (SMD) of 65–75 μm. Measurements of flow velocity and strain rate, as well as droplet size, axial velocity, and concentration over a range of nominal equivalence ratios are presented for comparison with the baseline prevaporized case. Reference laminar flame speeds (i.e., burning velocities) are reported as a function of strain rate, following the approach for gaseous reacting flows in which the laminar flame speed is directly proportional to the overall reaction rate [10–12]. Similar to our previous work [8], we measure the effect of fuel droplets on the strained laminar flame speed to understand their effect on the reaction rate. One-dimensional simulations of the gas phase and liquid phase are presented to complement the experimental data. The results and various complications arising from the experimental setup and the fate of droplets are discussed as follows.

2. Methods

2.1. Experimental setup

Fig. 1a shows the experimental setup, with acetone/air mixtures delivered from top and bottom burners. Nozzles converged the flow from a diameter of 71 mm to 14 mm over a 68 mm length to provide a top-hat velocity profile at the exit. The nozzle-to-nozzle distance was 24 mm ($L/D_n = 1.7$). Co-flow nitrogen was delivered through an annular channel of 10 mm gap to quench edge flames and suppress instabilities from the surrounding environment. Shielding air flow cooled the top burner

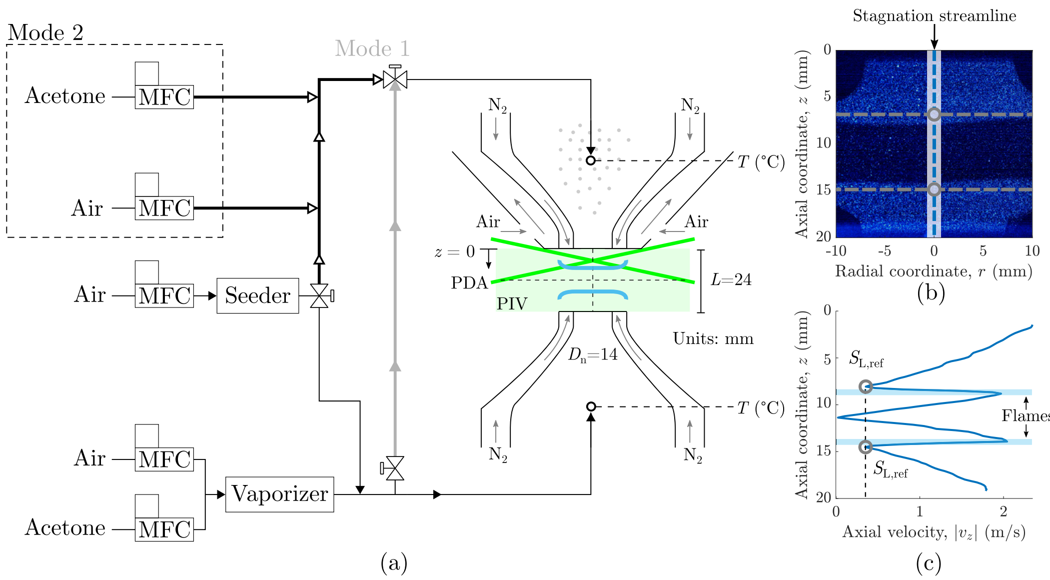

Fig. 1. (a) Experimental setup showing flow delivery to top and bottom streams in two modes. Mode 1 (gray arrows): prevaporized top and bottom mixtures; Mode 2 (open arrows): bottom prevaporized mixture, top dilute spray mixture. Valve symbols show how the flows are split for each mode. (b) Sample PIV image from which the axial velocity profile in (c) is extracted.

outer wall to partially suppress heat transfer from the flames to the top flow. Thermocouples (RS-Pro, Type K ±1.5 °C) were positioned 68 mm upstream of the nozzle exits. Ambient temperatures were monitored as 20 ± 5 °C.

Two counterflow modes were used. In Mode 1 (dual-prevaporized), prevaporized fuel was delivered through both the top and bottom nozzles, and each flow was controlled by a metering valve. In Mode 2 (prevaporized/spray), the fuel for the bottom mixture was prevaporized, while the fuel for the top mixture was injected as a dilute spray.

For Mode 1, air flow (Alicat Scientific, MCR-50SLPM) was supplied at a constant flow rate to the prevaporizing system to supply a vaporized fuel and air mixture to both burners evenly. A fine fuel mist was created using an air-blast atomizer (Delavan, AL-06), and injected into a cylindrical chamber heated to 150°C using heating tape (Omega, STH102-080). Air was bypassed accordingly and the mixture cooled to ambient temperature after vaporization. A second MFC (Alicat Scientific, MCR-250SLPM) fed air through a seeder (Texas Airsonics, AJ-1), varied according to the required total flow rate. The total flow was split evenly to supply seeded air to both burners. Needle valves positioned immediately upstream of each burner were used to ensure flow symmetry (verified using sample PIV-processed images). Flow rates through each air supply were verified using a mass flow meter (Sensirion, SFM4100). For Mode 2, a third mass flow controller (Alicat Scientific, MCR-250SLPM) supplied air directly to the top burner at the same flow rate as that supplied to the bottom prevaporizing system. The estimated uncertainty of the gas flow rate measurements was 1% based on the stated accuracy at full scale. Two high-precision liquid mass flow controllers (Bronkhorst, Coriolis M13) fed liquid acetone (Thermo Scientific Acros, purity: 99.9%) through the respective atomizers. An ultrasonic atomizer (Sono-Tek, 8700-120) was used to create a dilute spray for the top flame, injected at the inlet of the mixing chamber far upstream of the nozzle exit (z = -275 mm). The systematic uncertainty of the air mass flow rates for Mode 1 was approximated as 1% for the seeded air and vaporizing air, respectively; for Mode 2, the uncertainty for the additional air supplied to the top burner was also approximated as 1%. For the fuel mass flow rate, the estimated uncertainty was 0.2% for both modes, corresponding to the instrumentation accuracy. The nominal equivalence ratio accuracy, derived from the uncertainties associated with the air and fuel delivery, ranged from 1–2% for Mode 1 and 1.5–3% for Mode 2.

2.2. Operating conditions

Mixture compositions were characterized by the nominal equivalence ratio, ϕ_0, based on the ratio of measured total mass flow rates of air and fuel. For Mode 1, $\phi_0 = [0.8, 1.0, 1.2]$; for Mode 2, ϕ_0 ranged from 0.8–1.4, ascending in increments of 0.05. For each nominal equivalence ratio, measurements were made for nozzle exit velocities between 1.4–2.7 m/s for both top and bottom flows; this allowed a sufficiently wide range of strain rates to be studied ($K = 200 - 600\ \mathrm{s}^{-1}$) away from extinction, and excluding flames stabilized at the nozzle rim.

2.3. Gas phase measurements

The velocity fields were determined using PIV via a double-pulsed Litron Nano-PIV laser at 532 nm with a repetition rate of 10 Hz. The beam was shaped into a 1 × 24 mm^2 laser sheet. Images were captured using a 2048 × 2048 px^2 CCD camera (LaVision, Imager Pro X 4M) operating in double frame mode at 5 Hz. The camera was focused using a 2× magnification teleconverter (Sigma, 2x EX DG) and a 60 mm micro-lens (Nikon, Nikkor 60 mm f1/2.8 D). A 532 nm ± 0.5 nm bandpass filter was attached to the micro-lens to reduce background signal. The projected pixel size was 9.4 µm/px, as calibrated by a target plate. The field of view area was measured as 19.3 × 19.3 mm^2. Aluminium oxide powder (1 µm) served as the gas phase PIV tracer particle, with a Stokes number below 0.1. The time interval between the two laser pulses varied between 50 and 100 μs, descending with increased flow rate for optimal spatial resolution. A total of 300 PIV images were taken for every flow rate condition for statistical convergence. The PIV images were processed in DaVis 8.4 (LaVision) using a multipass cross-correlation algorithm. A constant upper intensity threshold omitted droplets greater than roughly 5 µm from the algorithm. To generate the velocity vector fields, a 64 × 64 px^2 interrogation window with a 50% overlap followed by a 32 × 32 px^2 interrogation window with a 50% overlap were used, resulting in a vector spacing of 150 µm and an interrogation region of 300 µm. Post-filtering, the average velocity error using this algorithm was 1 cm/s for Mode 1 and 3 cm/s for Mode 2.

The method developed in [10–12] was used to estimate the reference flame speed. The stagnation streamline (vertical dashed line in Fig. 1b) was obtained as the streamline along which the radial velocity is zero. The minimum axial velocity along this streamline ahead of the acceleration produced by each flame (gray circles in Fig. 1c) was assigned as the reference flame speed, $S_{\mathrm{L,ref}}$, for the top and bottom flows, respectively. The values obtained are a function of the strain rate, which was determined from the gradient of the radial velocity, a, via the relation $K = 2a$, localized radially around the stagnation streamline (horizontal dashed lines in Fig. 1b). The accuracy of the gradient was a function of the estimated velocity error and the resolution.

An automated filtering scheme was developed to discard invalid images, according to the following criteria: (A) steady-state; and (B) one-dimensional and axisymmetric. Images rejected owing to Criterion A were identified by local strain rates that deviated by more than one standard deviation from the mean (across 300 images), attributed mostly to poor seeding or asymmetric flame behavior. Criterion B ensured that flames exhibiting two-dimensional effects were rejected. Such flames were identified by estimating the variability in the axial velocity at radial positions within ±0.75 mm of the reference position (gray circles in Fig. 1b-c) for each flame. The ascribed tolerance (10%) was somewhat higher than that of our previous study [8] to account for fluctuations caused by the presence of larger droplets (> 20 µm). For each flow rate condition, at least 100 images were retained, ensuring sufficient statistical convergence.

2.4. Liquid phase measurements

Three parameters were measured to characterize the droplets: (a) size, represented by SMD (D_{32}, µm); (b) axial velocity (v_{d}, m/s); and (c) concentration (n_{d}, #/cm^3). These parameters were obtained using a Dantec Dynamics phase Doppler anemometry (PDA) system, consisting of a 514.5 nm laser, a 500 mm focal length transmitting probe, and a 310 mm focal length collecting probe positioned 20° off-axis from the forward scattering direction. An aperture mask constrained the maximum detectable particle diameter to roughly 161 µm. Two sets of measurements were obtained: non-reacting droplet measurements (5000 samples per case) were taken halfway between the top burner nozzle exit and the stagnation plane ($z = 6$ mm); reacting droplet measurements were taken along the stagnation streamline (z =6–11 mm), whereby the PDA system translated axially every 60 s. The data rates were of the order of 10^2 Hz for non-reacting measurements and 10^0–10^1 Hz for reacting measurements. The nominal equivalence ratios for these measurements ranged from 0.8–1.4.

3. Results and discussion

3.1. Droplet characteristics

The droplet Sauter mean diameter ranged between 65–75 µm; the variation, determined over the flow velocity range, was less than 10% for all mixtures. Fig. 2 shows the corresponding non-reacting droplet concentration estimates, and the inset shows a typical droplet size distribution. Typical size distributions for the range of mixtures are provided in the Supplementary Material (S1, Fig. S1.1).

The Stokes number (Stk) was calculated as the ratio of the characteristic droplet time scale ($\rho_{\mathrm{d}} D^2 [18(1+\frac{1}{6}\mathrm{Re}_{\mathrm{d}}^{0.67})\mu_{\mathrm{gas}}]^{-1}$) [13] to the characteristic flow time scale ($1/K$), where ρ_{d} is the liquid acetone density, Re_{d} is the Reynolds number based on the droplet diameter and the flow velocity, and μ_{gas} is

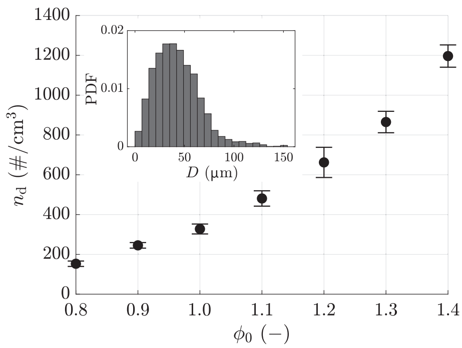

Fig. 2. Non-reacting droplet concentration (n_d) as a function of nominal equivalence ratio (ϕ_0), measured from downstream of the top burner nozzle at $z = 6$ mm. Error bars are based on the root mean square deviation relative to the mean, represented by the standard deviation. Inset: Normalized distribution of droplet diameter (D) for $\phi_0 = 1.2$ and $K = 400$ s^{-1}.

Table 1
Stokes number (Stk) estimates for non-reacting droplets in Mode 2 across a range of strain rates ($K =$ [200, 400, 600] s^{-1}) and droplet sizes (D =10–100 μm) at $\phi_0 = 1.2$. Measurements were taken at $z = 6$ mm, downstream of the top burner nozzle exit.

	Stk		
D (μm)	$K = 200$ s^{-1}	$K = 400$ s^{-1}	$K = 600$ s^{-1}
10	0.032	0.059	0.084
25	0.156	0.281	0.392
50	0.492	0.879	1.237
75	0.977	1.794	2.477
100	1.569	2.953	4.236

Table 2
Fuel liquid fraction (α_{liq}) and effective equivalence ratio (ϕ_e), estimated using the measurements of mean non-reacting droplet concentration (n_d) and droplet diameter for each nominal equivalence ratio (ϕ_0) at $z = 6$ mm.

ϕ_0 (–)	n_d (#/cm^3)	α_{liq} (%)	ϕ_e (–)
0.8	153	6.0	0.75
0.9	245	6.3	0.84
1.0	328	7.4	0.92
1.1	481	11.9	0.97
1.2	662	15.3	1.02
1.3	865	16.7	1.08
1.4	1196	22.0	1.09

the gas dynamic viscosity. Table 1 shows the variation in Stk as a function of droplet size and strain rate for $\phi_0 = 1.2$, measured in non-reacting conditions at a distance $z = 6$ mm from the top nozzle. The increased Stk with increased droplet size and strain rate suggest that significant slip is expected for large droplets as the flow decelerates into the flame.

Table 2 reports the mean non-reacting droplet concentration estimates for each nominal equivalence ratio at $z = 6$ mm. For each mixture, the liquid fraction (α_{liq}) and the effective equivalence ratio (ϕ_e) were calculated using the liquid flux method [14] and PDA measurements of size and concentration. These calculations are detailed in the Supplementary Material (S2). The liquid fraction varied from 6% at the leanest ϕ_0 to 22% at the richest ϕ_0. The estimated liquid fraction may differ from the actual value, as it is known that integration of the liquid flow rates extracted from droplet number concentrations can diverge from the actual total droplet flux concentrations in both evaporating and non-evaporating streams [15]. The discrepancy between the estimated effective equivalence ratio and the nominal equivalence ratio increases for nominally rich mixtures. This is a result of the decreased potential for vaporization as the vapor concentration increases and temperature decreases owing to evaporative cooling.

3.2. Strained flame speed

Fig. 3 shows the reference flame speed as a function of strain rate for $\phi_0 = [0.8, 1.0, 1.2]$ for two datasets corresponding to Mode 1 (fully vaporized) and Mode 2 (spray top, vapor bottom). Gray squares denote the bottom vapor flame data for Mode 1; measurements of the top flame are not shown, as they were susceptible to temperature increases caused by heat transfer of product gases. Open squares and circles denote the vapor and spray flame data, respectively, for Mode 2. Simulation results for the reference flame speed are also plotted, obtained from a Cantera [17] one-dimensional model using the chemical mechanism of Pichon et al. [16] at ambient conditions; the solid lines denote simulations for ϕ_0, while dashed lines denote simulations for the estimated effective equivalence ratio, ϕ_e, accounting for incomplete vaporization at the same temperature.

There is good agreement between the ϕ_0 model results and the Vapor (Mode 1, B) results for all three mixtures. This dataset represents the baseline against which the droplet-influenced Mode 2 flames are examined.

Fig. 3a shows that for $\phi_0 = 0.8$ in Mode 2 (open circles), the addition of droplets lowers the measured flame speed slightly relative to the fully vaporized case. The lower values are consistent with the lower effective equivalence ratio of 0.75 (Table 2), although the effect of droplets for $K < 300$ s^{-1} is greater than the simulations predict. However, it is difficult to explain the slightly steeper slope with strain at this range without corresponding baseline data from Vapor (Mode 1, B).

Fig. 3b shows that for $\phi_0 = 1.0$, the Spray (Mode 2, T) results are barely distinguishable from the baseline Vapor (Mode 1, B) results: here, a slight reduction in the flame speed would be expected, associated with an effective equivalence ratio of 0.92 (Table 2), but this offset could have been counter-

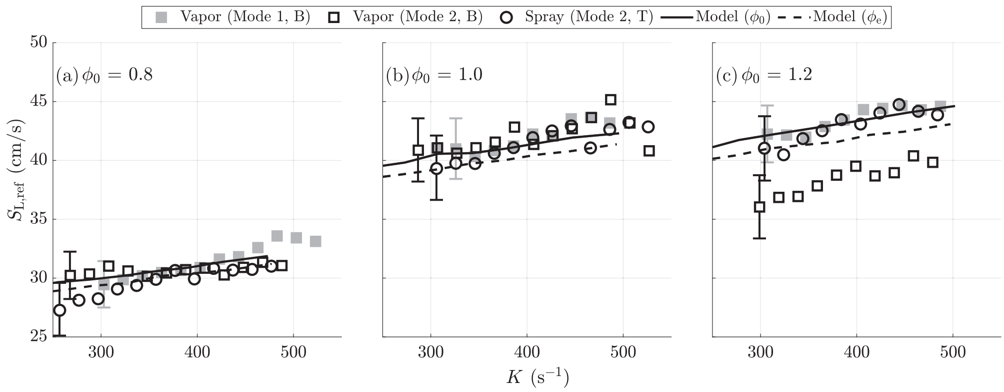

Fig. 3. Laminar flame speed ($S_{L,ref}$) as a function of strain rate (K) comparing measured datasets (Mode 1: gray symbols, Mode 2: open symbols) with gas phase simulation results (black solid and dashed lines), computed using the mechanism of Pichon et al. [16]. 'B' and 'T' denote bottom and top flows, respectively. Representative error bars correspond to the standard deviation at the respective strain rate. Inlet temperature: 20 °C.

acted by the slight heating of the incoming stream by the surrounding products, which was more pronounced at near-stoichiometric cases owing to elevated flame temperatures.

Finally, for the richer case in Fig. 3c ($\phi_0 = 1.2$), there again appears to be minimal difference between the Spray (Mode 2, T) results and the baseline results. A leaner mixture ($\phi_e = 1.02$) would be expected from the incomplete vaporization, according to Table 2; according to the model results for ϕ_e, the leaner mixture should lead to minimal change in the flame speed. Therefore, one cannot yet be certain of whether incomplete vaporization effects are dominant without direct measurements of the product composition. The Vapor (Mode 2, B) results show a distinct drop in reference flame speed relative to the baseline results, which surprisingly suggests that the bottom vapor flame may be influenced by the spray from the top stream, as addressed further on.

Fig. 4 shows similar information about the reference flame speed, but as a function of nominal equivalence ratio for a fixed strain rate ($K = 400$ s^{-1}). Comparing the baseline results (gray squares) with Spray (Mode 2, T) results (open circles), we see that the reference flame speed for the spray case is slightly lower than the baseline in the lean case and indistinguishable for the stoichiometric and rich cases. Comparing the spray case (open circles) with the model (dashed line), we notice that the spray measured values are slightly lower than the model calculations on the lean side, and either comparable or slightly higher on the rich side for $\phi_0 > 1.1$. This is consistent with the idea that the effective equivalence ratio is shifted to a lower value than nominal, as expected from Table 2. Finally, considering the Vapor (Mode 2, B) results (open squares), we see that the measured values are significantly lower than the values of both the spray case and the model on the rich side for $\phi_0 > 1.1$,

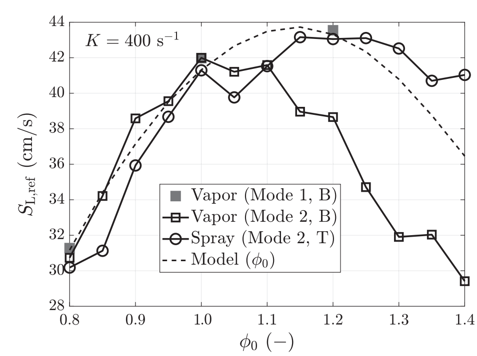

Fig. 4. Laminar flame speed ($S_{L,ref}$) as a function of nominal equivalence ratio (ϕ_0) at $K = 400$ s^{-1}, comparing measured datasets and simulation results. Symbol key as in Fig. 3. Model simulations were performed using the mechanism in [16] with an inlet temperature of 20 °C.

as seen also in Fig. 3c. The working hypothesis is that, for nominally rich mixtures, a high fraction of droplets from the top spray evades combustion and penetrates the bottom flame. This hypothesis is investigated in the following sections.

3.3. Flame emission

Fig. 5 depicts natural light images of the Mode 2 flame structures for $\phi_0 = [0.8, 1.0, 1.2]$ at $K = 400$ s^{-1}. The images were obtained using a DSLR camera (Nikon, D7000) with a 50 mm lens (Nikon, Nikkor 50 mm f/1.8 D) at an exposure time of 1/25 s, ISO100, and aperture 1.8. The images were taken during exposure to the PIV laser light.

The chemiluminescence of the lean and stoichiometric flames (Fig. 5a-b) is not greatly affected by the presence of droplets, even though large droplets (green dots) are visible in all images.

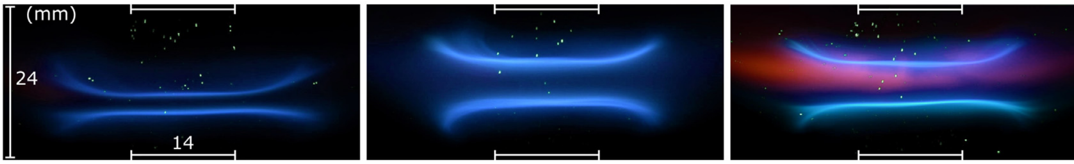

(a) $\phi_0 = 0.8$ (b) $\phi_0 = 1.0$ (c) $\phi_0 = 1.2$

Fig. 5. Natural light images of lean (a), stoichiometric (b), and rich (c) flames (Mode 2) corresponding to $K = 400$ s^{-1}. Green dots are droplets illuminated by a 1×24 mm^2 laser sheet formed using the double-pulsed PIV laser (532 nm, 10 Hz).

For $\phi_0 = 1.2$ (Fig. 5c), the vapor flame emits a green tinge, characteristic of C_2^*, while the spray flame retains a light blue hue, characteristic of CH^*, and features an orange emission band, possibly caused by CO^* or soot.

The images show droplets *crossing* the flame for all mixtures, especially at $\phi_0 = 1.2$ (Fig. 5c). This has significant implications for both flames: for the top spray flame, it implies a *lower* equivalence ratio due to incomplete vaporization; for the bottom vapor flame, it possibly implies a *higher* equivalence ratio due to the additional fuel supplied by droplets, and a possible reduction in the adiabatic flame temperature due to the enthalpy required for droplet evaporation.

3.4. Droplet behavior along the stagnation streamline: Measurements and simulations

Fig. 6 shows the mean gas phase velocity profiles (black solid and dashed lines) as well as corresponding liquid phase PDA measurements along the stagnation streamline for a rich case ($\phi_0 = 1.2$, $K = 400$ s^{-1}). The gas velocity profiles differ between Modes 1 and 2. On the spray side, the profiles are slightly offset, possibly owing to the cooling effect of droplets (the measured temperature of the top mixture for the vapor Mode 1 case is 35 °C, compared to 25 °C for the spray Mode 2 case). We note also that the top flows are both affected by the heat transfer of product gases. More importantly, we observe roughly the same velocity rise on the top flow side for both modes, but a much lower rise on the bottom flow side for Mode 2. This suggests a higher flame temperature on the spray side compared to the vapor side, which suggests that the effective equivalence ratio of the flame on the bottom vapor side may be *higher*, i.e., *richer* than the nominal value. The gas velocity rise on the top spray side could correspond to either the nominal equivalence ratio (1.2) or the effective equivalence ratio (1.02), as the burned gas temperature is not significantly different between those two cases (within 30 °C, according to the gas phase simulations), which would result in similar velocity rises.

The droplet counts (triangles) decrease significantly across the flame as vaporization occurs, as expected. Owing to an increase in temperature of the incoming mixture from the top after a few minutes, it was not possible to obtain reliable concentration estimates. Future measurements will incorporate more cooling to allow longer measurement intervals. Nevertheless, the results indicate a slight increase in SMD (squares) across the flame, suggesting that small droplets evaporate, while larger droplets traverse the flame zone. Liquid velocities (open circles), denoting the mean droplet velocities, show significant slip relative to the gas velocities, illustrating their survival across the flame.

The findings discerned from the streamline measurements were complemented by parametric one-dimensional liquid phase simulations for droplets crossing from the top flow into the opposing flow along the center streamline, starting from the stagnation plane. Equations of motion, mass, and temperature were solved for independent single droplets considering gravity, buoyancy, the Schiller-Naumann correlation [18] for aerodynamic drag, and the Abramzon and Sirignano model [19] for the effects of Stefan flow on heat and mass trans-

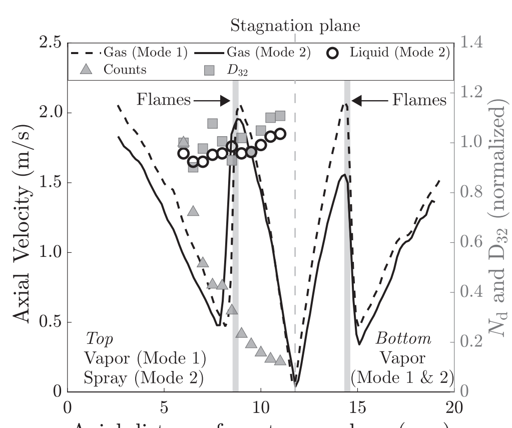

Fig. 6. Representative mean gas phase axial velocity for Modes 1 and 2 ($|v_z|$, derived from averaged PIV images) overlaid with corresponding Mode 2 liquid phase properties along the stagnation streamline ($\phi_0 = 1.2$, $K = 400$ s^{-1}, $D_{32} = 66.0$ µm ± 1.9 µm, Stk ≈ 1.5). Left axis (black): axial velocity (m/s); Right axis (gray): Droplet counts (N_d) and size (D_{32}), normalized by their respective initial values.

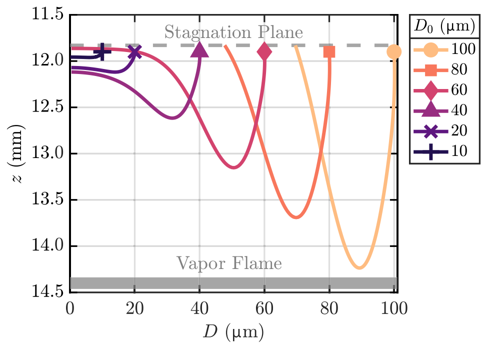

Fig. 7. Representative state space of simulated axial coordinate (z) for hypothetical droplets with initial diameters $D_0 = 10$–100 μm and initial axial velocities of 1.80–2.16 m/s. Gas phase properties derive from simulations for $\phi_0 = 1.2$ and $K = 400$ s^{-1}, computed using the mechanism in [16]. The initial position for each droplet diameter is illustrated by their respective symbol.

fer between uniform temperature droplets and the surrounding gas. Two-way momentum and energy coupling between phases was neglected, but the aforementioned Cantera simulations provided a realistic representation of the underlying gas phase velocity, species, and temperature profiles. The liquid phase simulations allowed for an estimation of the distance-droplet history of individual droplets starting with different initial diameters (D_0) and axial velocities (obtained from PDA measurements), as shown in Fig. 7.

Droplets above 10 μm decelerate, stagnate, and are then advected back towards the stagnation plane before fully evaporating. This suggests that the drag imposed by the vapor flame prevents droplet penetration, overcoming the pronounced initial slip motion. The droplet return is consistent with predictions in previous studies (e.g., [5,20,21]), although radial motion was not considered in the present study. Interestingly, the simulations imply that droplets penetrating the spray flame are likely to evaporate before reaching the vapor flame, and would contribute to lowering the temperature rise of the bottom vapor flame, as observed in Fig. 6.

4. Conclusions

The effect of fuel droplets on the burning velocity of strained laminar premixed flames was examined. Using the canonical counterflow configuration, gas phase flame speeds were measured as a function of strain rate for opposing prevaporized and droplet-laden acetone/air flames simultaneously over a range of nominal equivalence ratios. The mean droplet size (SMD) ranged from 65–75 μm, and the liquid fraction, determined by the natural atomization and evaporation process, ranged from 6–22%, as a monotonically increasing function of nominal equivalence ratio. These measurements were complemented by one-dimensional gas phase and liquid phase simulations.

The study provides the following insights on the effect of droplets on strained laminar flames in this particular configuration: (i) incomplete fuel vaporization causes a vapor fuel *deficit* for the affected flame, and the resulting flame speed is consistent with a leaning out of the overall mixture: lower for lean mixtures, and higher for richer mixtures; (ii) residual droplets with sufficiently high Stokes numbers may cross the stagnation plane, leading to a fuel *surplus* relative to the original nominal value, causing a reduction in adiabatic flame temperature and a richer product or reactant zone.

The simple framework of the opposed strained flames is useful for considering the systematic presence of droplets, but additional technical improvements are needed to allow better control of droplet size and liquid fraction. Further work is currently underway to improve on the original idea by providing further measurements of gas phase mixture fraction and temperature, and to better control the temperature of the incoming streams.

Declaration of Competing Interest

The authors declare that they have no known competing financial interests or personal relationships that could have appeared to influence the work reported in this paper.

Acknowledgments

The authors gratefully acknowledge C. T. Chong, M. Kuvshinov, A. Skiba, P. M. Allison, P. M. de Oliveira, M. P. Sitte, and Z. Chen for their insights. Equipment used in the present campaigns were shared with UK EPSRC grants EP/T015845/1 and EP/K035282/1. Initial work on the topic was funded by a Royal Society Newton Advanced Fellowship (NA160115) to C. T. Chong.

Supplementary materials

An interactive data visualization site accompanying this article can be found at [https://dmcgrath1.shinyapps.io/combustion/].

Supplementary material associated with this article can be found, in the online version, at 10.1016/j.proci.2022.07.133.

References

[1] S. Hayashi, S. Kumagai, T. Sakai, Propagation velocity and structure of flames in droplet-vapor-air mixtures, Combust. Sci. Technol. 15 (5–6) (1977) 169–177.

[2] H. Nomura, M. Koyama, H. Miyamoto, Y. Ujiie, J. Sato, M. Kono, S. Yoda, Microgravity experiments of flame propagation in ethanol droplet-vapor-air mixture, Proc. Combust. Inst. 28 (2000) 999–1005.

[3] D.R. Ballal, A.H. Lefebvre, Flame propagation in heterogeneous mixtures of fuel droplets, fuel vapor and air, Symp. (Int.) Combust. 18 (1981) 321–328.

[4] H.K. Chelliah, Flame inhibition/suppression by water mist: droplet size/surface area, flame structure, and flow residence time effects, Proc. Combust. Inst. 31 (2007) 2711–2719.

[5] R.J. Kee, K. Yamashita, H. Zhu, A.M. Dean, The effects of liquid-fuel thermophysical properties, carrier-gas composition, and pressure, on strained opposed-flow non-premixed flames, Combust. Flame 158 (6) (2011) 1129–1139.

[6] B. Franzelli, A. Vié, M. Ihme, On the generalisation of the mixture fraction to a monotonic mixing-describing variable for the flamelet formulation of spray flames, Combust. Theor. Model. 19 (6) (2015) 773–806.

[7] A. Neophytou, E. Mastorakos, Simulations of laminar flame propagation in droplet mists, Combust. Flame 156 (8) (2009) 1627–1640.

[8] L. Fan, B. Tian, C.T. Chong, M.N.M. Jaafar, K. Tanno, D. McGrath, P.M. de Oliveira, B. Rogg, S. Hochgreb, The effect of fine droplets on laminar propagation speed of a strained acetone-methane flame: experiment and simulations, Combust. Flame 229 (2021) 111377.

[9] L. Fan, C.T. Chong, K. Tanno, D. McGrath, Y. Zheng, S. Hochgreb, Measurement of the effect of water droplets on strained laminar flames using two-phase PIV, Proc. Combust. Inst. 38 (2021) 3183–3192.

[10] C.K. Wu, C.K. Law, On the determination of laminar flame speeds from stretched flames, Symp. (Int.) Combust. 20 (1985) 1941–1949.

[11] C.K. Law, D.L. Zhu, G. Yu, Propagation and extinction of stretched premixed flames, Symp. (Int.) Combust. 21 (1988) 1419–1426.

[12] D.L. Zhu, F.N. Egolfopoulos, C.K. Law, Experimental and numerical determination of laminar flame speeds of methane/(Ar, N2, CO2)-air mixtures as function of stoichiometry, pressure, and flame temperature, Symp. (Int.) Combust. 22 (1989) 1537–1545.

[13] S.C. Li, Spray stagnation flames, Prog. Energy Combust. Sci. 23 (4) (1997) 303–347.

[14] J.D. Gounder, A. Kourmatzis, A.R. Masri, Turbulent piloted dilute spray flames: flow fields and droplet dynamics, Combust. Flame 159 (11) (2012) 3372–3397.

[15] C.T. Chong, S. Hochgreb, Effect of atomizing air flow on spray atomization of an internal-mix twin-fluid atomizer, Atomization and Sprays 25 (8) (2015) 657–673.

[16] S. Pichon, G. Black, N. Chaumeix, M. Yahyaoui, J.M. Simmie, H.J. Curran, R. Donohue, The combustion chemistry of a fuel tracer: Measured flame speeds and ignition delays and a detailed chemical kinetic model for the oxidation of acetone, Combust. Flame 156 (2) (2009) 494–504.

[17] D.G. Goodwin, R.L. Speth, H.K. Moffat, B.W. Weber, Cantera: An object-oriented software toolkit for chemical kinetics, thermodynamics, and transport processes, 2021, (https://www.cantera.org). Version 2.5.1. doi:10.5281/zenodo.4527812.

[18] L. Schiller, A. Naumann, A drag coefficient correlation, Zeit. Ver. Deutsch. Ing. 77 (1935) 318–320.

[19] B. Abramzon, W.A. Sirignano, Droplet vaporization model for spray combustion calculations, Int. J. Heat Mass Transfer 32 (9) (1989) 1605–1618.

[20] N.-H. Chen, B. Rogg, K.N.C. Bray, Modelling laminar two-phase counterflow flames with detailed chemistry and transport, Symp. (Int.) Combust. 24 (1992) 1513–1521.

[21] A.M. Lentati, H.K. Chelliah, Dynamics of water droplets in a counterflow field and their effect on flame extinction, Combust. Flame 115 (1–2) (1998) 158–179.